

# D-Unet: A Dual-encoder U-Net for Image Splicing Forgery Detection and Localization

Xiuli Bi, Yanbin Liu, Bin Xiao, Weisheng Li, *Member, IEEE*, Chi-Man Pun, *Senior Member, IEEE*, Guoyin Wang, *Senior Member, IEEE*, and Xinbo Gao, *Senior Member, IEEE*

arXiv:2012.01821v1 [cs.CV] 3 Dec 2020

**Abstract**—Recently, many detection methods based on convolutional neural networks (CNNs) have been proposed for image splicing forgery detection. Most of these detection methods focus on the local patches or local objects. In fact, image splicing forgery detection is a global binary classification task that distinguishes the tampered and non-tampered regions by image fingerprints. However, some specific image contents are hardly retained by CNN-based detection networks, but if included, would improve the detection accuracy of the networks. To resolve these issues, we propose a novel network called dual-encoder U-Net (D-Unet) for image splicing forgery detection, which employs an unfixed encoder and a fixed encoder. The unfixed encoder autonomously learns the image fingerprints that differentiate between the tampered and non-tampered regions, whereas the fixed encoder intentionally provides the direction information that assists the learning and detection of the network. This dual-encoder is followed by a spatial pyramid global-feature extraction module that expands the global insight of D-Unet for classifying the tampered and non-tampered regions more accurately. In an experimental comparison study of D-Unet and state-of-the-art methods, D-Unet outperformed the other methods in image-level and pixel-level detection, without requiring pre-training or training on a large number of forgery images. Moreover, it was stably robust to different attacks.

**Index Terms**—Image splicing forgery detection, Tampered region localization, Convolutional neural network, Dual-encoder, Image fingerprints, Global perspective.

## I. INTRODUCTION

**D**ISCRIMINATING between a tampered and non-tampered image is a challenging task in modern times, because powerful image processing software and applications can easily manipulate images while leaving no visual clues of the manipulation. Therefore, confirming the authenticity of an image is an increasingly critical research topic. Depending on whether the semantic content of the image is changed or unchanged, image forgery is roughly divisible into two categories: global forgery and local forgery. Global forgery

This work was partly supported by the National Key Research and Development Project (2016YFC1000307-3), the National Natural Science Foundation of China (61806032 and 61976031), the Scientific & Technological Research Program of Chongqing Municipal Education Commission (KJQN201800611), the Chongqing Research Program of Application Foundation & Advanced Technology (cstc2018jcyjAX0117) and the Scientific & Technological Key Research Program of Chongqing Municipal Education Commission (KJZDK201800601). (Corresponding authors: Bin Xiao.)

Xiuli Bi, Yanbin Liu, Bin Xiao, Weisheng Li, Guoyin Wang and Xinbo Gao are with the Department of Computer Science and Technology, Chongqing University of Posts and Telecommunications, Chongqing, China. email: bixl@cqupt.edu.cn, S180231931@stu.cqupt.edu.cn, xiaobin@cqupt.edu.cn, liws@cqupt.edu.cn, wanggy@ieee.org, gaoxb@cqupt.edu.cn.

Chi-Man Pun is with the Department of Computer and Information Science, University of Macau, Zhuhai, Macau. email: cmpun@umac.mo.

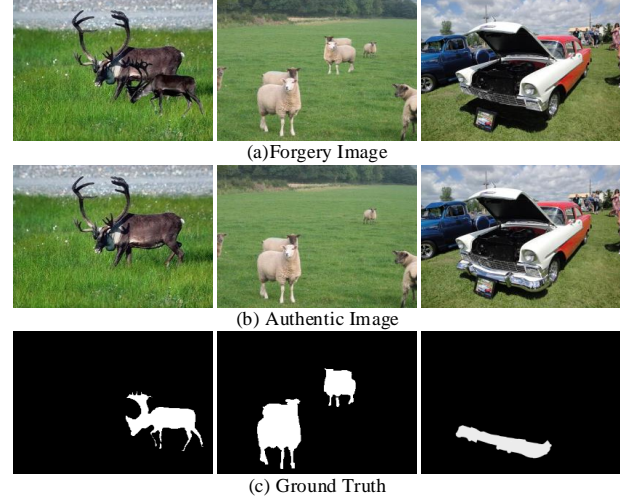


Fig. 1. Examples of image local forgery. The first, second and third columns show an image formed by splicing forgery, an image formed by a copy-move forgery, and an image formed by a removal forgery, respectively. Rows *a*, *b* and *c* display the forgery image, the authentic image and the ground truth, respectively.

is considered less harmful because it changes only the visual effect of the image (by techniques such as image compression, image blurring, and image contrast enhancement), without altering the semantic content. On the contrary, a local forgery alters the semantic content of the image, as shown in Fig. 1. Because a local forgery can propagate false or misleading information through the manipulated content, it is more harmful in different situations than global forgery. From the local the local forgery technique, copy-move and removal forgery require a single source image, but splicing forgery copies and pastes regions from one or more source images onto the target image (1<sup>st</sup> column of Fig. 1). The present paper focuses on detecting the tampered regions in splicing-forged images.

All images possess intrinsic properties caused by imaging processing or post-processing. As these intrinsic properties are unrelated to the image contents, they can be exploited for differentiating an image from any other image. For this reason, they are called *image fingerprints*. In splicing forgery images, the tampered and non-tampered regions come from different source images; accordingly, a splicing forgery can be detected by checking for different image fingerprints in different regions of an image. During the last decade, two main categories of image-fingerprint detection have been proposed: those based on traditional feature extraction, and those based on convolutional neural networks (CNNs). Many traditional detection methods extract the particular image fingerprints,

such as image-compression attributes [1–3], camera characteristics [4], edge inconsistencies [5, 6], and photo-response nonuniformity noise [7, 8]. Because they target one fingerprint, such methods fail when the targeted fingerprint is missing or non-obvious. Moreover, the particular image fingerprint will be affected by post-processing effects such as image blurring, JPEG compression and down-sampling, which degrades the detection results of traditional detection methods.

The use of CNNs in image-splicing forgery detection was inspired by the huge success of CNNs in computer vision. Table I summarizes the notable CNN-based detection methods for image splicing forgery proposed since 2016. In the table, these methods are distinguished by their ways: (1) how to consider image splicing forgery detection; (2) how to learn image fingerprints.

TABLE I  
SUMMARY OF CNN-BASED IMAGE FORGERY DETECTION METHODS  
THAT REALIZE PIXEL-LEVEL LOCALIZATION (BLUE FONT) OR PERFORM  
IMAGE-LEVEL CLASSIFICATION (BLACK FONT).

How to consider the image splicing forgery detection		
	Based on patch	Based on image
How to learn image fingerprints Autonomous	<p>Zhang, <i>et al.</i> [9](2016) Wei, <i>et al.</i> [10](2018) Xiao, <i>et al.</i> [11](2020)</p>	<p>Bayar, <i>et al.</i> [12](2016) Bayar, <i>et al.</i> [13](2018) Salloum, <i>et al.</i> [14](2018) Bi, <i>et al.</i> [15](2019)</p>
How to learn image fingerprints Intentional	<p>Rao, <i>et al.</i> [16](2016) Bappy, <i>et al.</i> [17](2017) Shi, <i>et al.</i> [18](2018) Liu, <i>et al.</i> [19](2020)</p>	<p>Zhou, <i>et al.</i> [20](2018) Bappy, <i>et al.</i> [21](2019) Wu, <i>et al.</i> [22](2019)</p>

Some researchers [9–11, 16–19] have regarded image splicing forgery detection as a binary classification of the image patches. As these detection networks focus only on the local patches and ignore the relationship between the image patches, they easily return false decisions. For example, an image patch in the tampered regions will be predicted as a non-tampered patch because it has the same extracted image fingerprints. Moreover, as the final detection results are derived from the decisions of image patches, the detected regions are generally composed of square white blocks, or the boundaries of the tampered regions. To resolve these problems, some researchers [12–15, 20–22] have employed end-to-end networks, which handle the image splicing forgery detection as an image segmentation or object detection task. As these methods consider the contextual relationships between local patches, they tend to outperform the patch-wise detection networks. In fact, image splicing forgery detection is a global binary classification task that distinguishes between tampered and non-tampered regions. Especially, a single splicing forgery image includes multiple tampered regions, so the decisions of the detection network must cover local regions and local objects. However, the existing detection methods usually target either local patches or local objects, which is insufficient for high-performance detection of splicing forgery.

For autonomous learning image fingerprints, some detection methods [9–15] have exploited the learning ability of CNNs or re-deployed existing CNNs originally proposed for other tasks. Whereas some researchers [16–19] have employed CNNs only for learning a particular image fingerprint, others [20–22] have strengthened the autonomous learning of image fingerprints using a particular image fingerprint. Although these CNN-based detection methods have demonstrated high-performance learning of image fingerprints, their accuracy would be improved by considering specific image contents. For example, the direction information of the pixels, which represents the boundaries of tampered regions, is an important trail but is almost ignored by CNNs. Although a smattering of detection methods [18, 21] have considered the specific contents of images, they do not fully explore the cooperation of the specific image contents with the image fingerprints learned by CNNs, which partially explains their non-promising detection results.

In summary, the existing CNN-based detection methods have not yet achieved the expected performance, and generally need a pre-training process or training on a large number of training samples as listed in Table II. The low performance of these methods can be attributed to two aspects that have not been fully considered: the intrinsic characteristic of image splicing forgery, and the learning of image fingerprints. To resolve these issues, we propose a novel network called dual-encoder U-Net (D-Unet) for splicing forgery detection. Our main contributions are summarized below.

TABLE II  
NUMBERS OF SAMPLES IN THE TRAINING/PRE-TRAINING PROCESSES OF  
EXISTING CNN-BASED DETECTION METHODS FOR IMAGE SPLICING  
FORGERY.

Method	Pre-training	Training set
Rao, <i>et al.</i> [16]	No	16K(patch)
Zhang, <i>et al.</i> [9]	No	100K(patch)
Bappy, <i>et al.</i> [17]	No	100K(patch)
Wei, <i>et al.</i> [10]	No	335K(patch)
Bayar, <i>et al.</i> [12]	No	600K(patch)
Bayar, <i>et al.</i> [13]	No	600K(patch)
Bi, <i>et al.</i> [15]	No	4K(image)
Shi, <i>et al.</i> [18]	No	50K(patch)
Salloum, <i>et al.</i> [14]	No	5K(image)
Xiao, <i>et al.</i> [11]	No	335K(patch)
Liu, <i>et al.</i> [19]	No	160K(patch)
Zhou, <i>et al.</i> [20]	Yes	42K(image)
Bappy, <i>et al.</i> [21]	Yes	65K(image)
Wu, <i>et al.</i> [22]	Yes	1.25M(patch)
Ours	No	1K(image)

- Global perspective: we regard the image splicing forgery detection as a global binary classification of the splicing forgery image. Based on the end-to-end D-Unet, we construct a spatial pyramid global-feature extraction module (SPGFE) that expands the global insight further, which

achieves better detection performance than the existing methods.

- Dual-encoder: we employ an unfixed encoder that autonomously learns the image fingerprints and a fixed encoder that intentionally provides the direction information of the pixels to each stage of the detection network. The image fingerprints and pixel directions cooperate to enhance the learning and locating processes of the detection network.
- Reduced number of training samples: Owing to its structure, D-Unet gains insight into the image splicing forgery under the global perspective. Therefore, it achieves promising performance without requiring a large number of training samples and a pre-training step.

The remainder of this paper is organized as follows. Section II introduces the existing CNN-based detection methods for image forgery detection. Section III briefly presents the proposed D-Unet, and then introduces the dual-encoder structure and SPGFE module. Section IV assesses the detection performances of the proposed D-Unet and (for comparison) state-of-the-art detection methods. The paper concludes with Section V.

## II. RELATED WORK

As summarized in Table I, some of the proposed detection networks classify only whether an image is original or has been tampered. Rao, *et al.* [16] replaced the first layer of a visual geometry group (VGG) with a steganalysis rich model (SRM) [23] to obtain the image noise fingerprint of the input image. Whether the image had been tampered or not was then assessed by a VGG network. Bayar, *et al.* [12, 13] designed a constrained convolution layer that suppresses the image contents and adaptively learns the forgery features. After training on 10 different datasets, their network detected multiple types of image global forgery. Zhou, *et al.* [20] introduced Faster Region-CNN with an SRM layer that extracts the image noise fingerprint, providing additional evidence for the classification of multiple types of image local forgery.

Other detection networks focus on locating the tampered regions. Zhang, *et al.* [9] utilized a three-layer CNN with a multi-layer perceptron (MLP). Wei, *et al.* [10] proposed a two-stage VGG network, and Xiao, *et al.* [11] designed a two-stage network that locates the tampered regions on both coarse and refined scales, and generates the final detected tampered regions by an adaptive clustering approach. These three methods [9–11] are performed on image patches, which causes high computational complexity. Moreover, their detection results are either inaccurate or require complex post-processing. Salloum, *et al.* [14] proposed a multi-task FCN (MFCN) with two output branches for multi-task learning. One branch learns the tampered regions, while the other branch learns the boundaries of the tampered regions. Bi, *et al.* [15] presented a ringed residual U-Net (RRU-Net), in which the ringed-residual structure is formed from residual-propagation and residual-feedback modules. The RRU-Net structure enhances the feature propagation and encourages feature reuse. Both MFCN and RRU-Net [14, 15] are difficult to train and the

detection results could be further improved. Bappy, *et al.* [17] inserted a long short-term memory (LSTM) network between the second and third layers of a five-layer CNN for learning the spatial correlations among the non-overlapping image patches. Shi, *et al.* [18] extracted the image noise fingerprint by an SRM layer, then employed a VGG network that learns the differences between the tampered and non-tampered regions. Finally, the tampered regions with the help of 7 statistical features calculated in the frequency domain based on [9], the tampered regions are detected. Liu, *et al.* [19] extracted the noise and JPEG compression features by DenseNet, and hence located the tampered regions. However, these three methods [17–19] learn only a particular image fingerprint, and easily obtain false decisions. Bappy, *et al.* [21] extracted the resampling features by a Laplacian filter and LSTM, and obtained the spatial domain features by an encoder-decoder network. The resampling and spatial domain features were then fused to locate the tampered regions. Wu, *et al.* [22] presented an image manipulation trace-feature extractor and a local anomaly detection network. The methods of Bappy, *et al.* [21] and Wu, *et al.* [22] attempt to strengthen the autonomous learning of image fingerprints by a particular image fingerprint, but the pre-training requires many forged samples to improve the detection results. The above-mentioned detection methods locate only the tampered regions, and cannot directly classify the forgery and original images; instead, image-level classification is realized by artificially setting a threshold of the detected regions.

## III. THE PROPOSED DUAL-ENCODER UNET

Our proposed dual-encoder U-Net (D-Unet) (as shown in Fig. 2) locates the tampered regions in splicing forgery images. Utilizing the powerful feature learning and mapping abilities of CNNs, the unfixed encoder of D-Unet autonomously learns the image fingerprints that distinguishes the tampered and non-tampered regions. The fixed encoder extracts the direction information of the pixels in the image, and cooperates with the unfixed encoder during the learning and decision-making of the detection network. Next, the global insight of D-Unet is expanded by a SPGFE, which obtains low-resolution feature maps with global features. Finally, the decoder learns the mapping from the low-resolution feature maps, and makes pixel-wise predictions of the tampered regions. Owing to its structure, D-Unet gains insights into the image splicing forgery under a global perspective; accordingly, it maintains steady performance when detecting different cases of splicing forgeries, without requiring a large number of training samples or a pre-training process. In the subsequent subsections, we describe the unfixed encoder, fixed encoder, and SPGFE module of the proposed D-Unet in detail.

### A. The Unfixed Encoder in Dual-encoder of D-Unet

To effectively utilize the feature learning and mapping ability of CNNs in the CNN-based detection method for image splicing forgery, we must analyze the intrinsic characteristics of image splicing forgery in advance. Based on the similarity of the tampered regions to their surrounding regions, splicing forgery can be generally divided into object splicing forgery

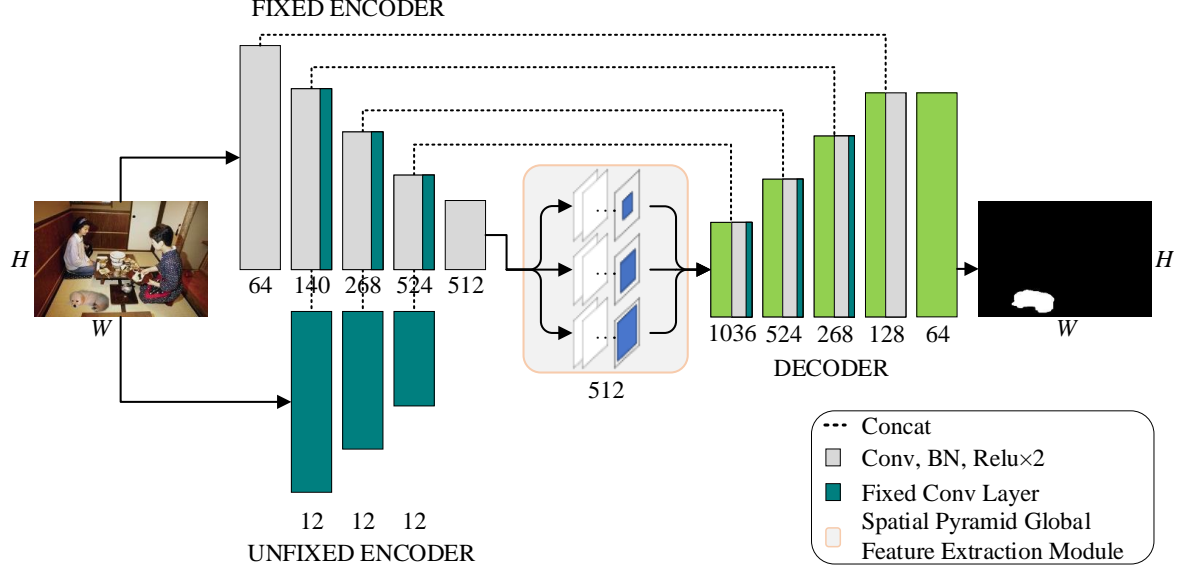


Fig. 2. Structure of the proposed D-Net.

and smooth splicing forgery. If the tampered and surrounding regions are similar, the boundaries of the tampered regions are indistinct. Methods that distinguish between tampered and non-tampered regions mainly detect the differences in the image fingerprints of both types of regions. If the tampered regions are objects, their boundaries will introduce real edges in splicing forgery images. In this case, the direction information of the pixels is an important addition to the image fingerprints. Because image fingerprints are necessary in both cases of splicing forgery, learning the image fingerprints is the foremost task of forgery-detection networks.

When learning the image fingerprints that distinguish tampered from non-tampered regions, the network depth must be carefully chosen because the image fingerprints generally possess basic image properties rather than high-level semantic features. A deep network learns the higher-level semantic information and loses the basic image properties. Conversely, the learned features of a shallow network are insufficient for exploring the different image fingerprints of the tampered and non-tampered regions. The way of down-sampling in the detection network is also important. The forgery prediction of the decoder is based on the low-resolution feature maps that contain the differences between the image fingerprints. To distinguish between the tampered and non-tampered regions, the image fingerprints must be maintained and even enhanced. Down-sampling by max-pooling retains the most representative features in the current feature maps. As the image fingerprints are less representative, it can be reduced or missed.

As the basic network in the proposed D-Net, we employ U-Net [24] because it delivers promising performance on image semantic segmentation. To analyze the effect of the network depth and down-sampling operation, we vary the depth of U-Net and performed down-sampling by a convolution of stride 2 or max-pooling. The experiments are carried out on two public datasets, CASIA [25] and [4]. The CASIA dataset [25] includes 750 splicing forgery images for training and

validation sets, and 100 splicing forgery images for the testing set. The COLUMB dataset [4] includes 135 splicing forgery images for the training and validation sets, and 45 splicing forgery images for the testing set. The U-Nets with max-pooling and stride-2 convolution down-sampling are denoted by Unet-N-M, and Unet-N-C, respectively. The number N in the middle part of the name represents the number of down-sampling operations in the encoder part of U-Net.

For a subjective analysis, we select two splicing forgery images from the testing sets, and evaluate their results in different cases of U-Net. As shown in Fig. 3. Regardless of whether the tampered regions are similar to their non-tampered surroundings (Fig. 3-(a1)), or are objects inserted into the image (Fig. 3-(a3)), U-Net with depth 4 achieves the best detection result on both cases. Moreover, U-Nets of the same depth consistently achieve higher performance when down-sampled by a convolution of stride 2 than when down-sampled by max-pooling. For objective evaluation, the detection results of the U-Net variants on both datasets are compared in Table III. Again, Unet-4-C still shows the best performance. The experimental results verify the importance of selecting a suitable network depth and down-sampling operation. In subsequent analyses, we employ Unet-4-C as the unfixed encoder and decoder in the proposed D-Net.

#### B. The Fixed Encoder in Dual-encoder of D-Net

The unfixed encoder autonomously learns the image fingerprints that differentiate between the tampered and non-tampered regions, as shown in the experimental results of Unet-4-C in subsection III-A. However, in some state-of-the-art CNN-based detection methods for image splicing forgery, the detection networks [16–19] only learn the particular image fingerprint, whereas others [20–22] attempt to strengthen the autonomous learning of networks by learning a particular image fingerprint. The particular image fingerprint, which generally exists in images, is thought to directly improve the learning effectiveness of the detection network.

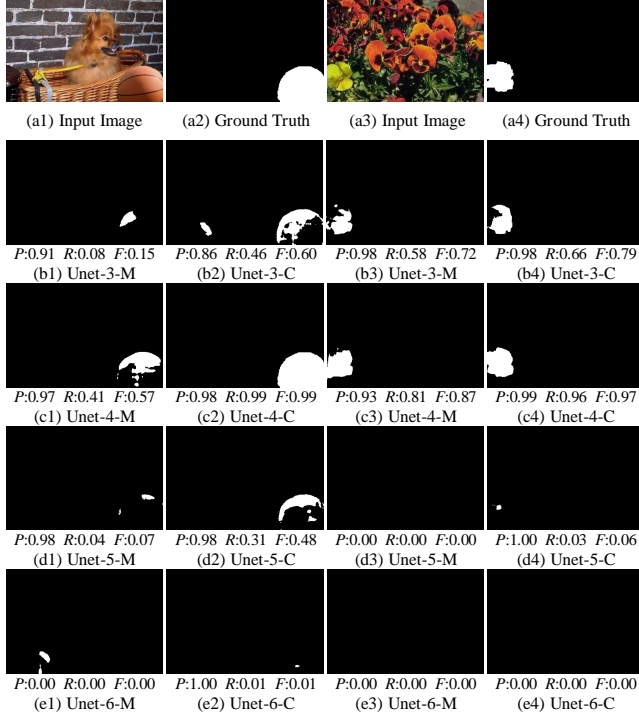


Fig. 3. Regions of two splicing forgery images, detected by U-Nets with different depths and down-sampling operations. Shown are the splicing forgery images and their ground-truth masks (row a) and the detection results of Unet-3, Unet-4, Unet-5, and Unet-6 (row b, c, d, and e, respectively). Column a1 and a3 are the detection results of max-pooling, and column a2 and a4 are the detection results of stride-2 convolution.

TABLE III

DETECTION RESULTS OF U-NETS WITH DIFFERENT NETWORK DEPTHS AND DOWN-SAMPLING OPERATIONS ON THE CASIA AND COLUMB DATASETS.

Method	Detection Result					
	CASIA			COLUMB		
	Precision	Recall	F	Precision	Recall	F
Unet-3-M	0.795	0.736	0.765	0.832	0.43	0.567
Unet-4-M	<b>0.815</b>	0.735	0.773	0.906	0.535	0.661
Unet-5-M	0.794	0.722	0.756	0.853	0.502	0.632
Unet-6-M	0.729	0.639	0.681	0.849	0.487	0.619
Unet-3-C	0.801	0.76	0.78	0.835	0.531	0.649
Unet-4-C	0.813	0.764	<b>0.788</b>	<b>0.923</b>	<b>0.547</b>	<b>0.686</b>
Unet-5-C	0.774	<b>0.782</b>	0.778	0.866	0.538	0.664
Unet-6-C	0.752	0.648	0.696	0.848	0.525	0.649

For this issue, we construct a fixed SRM encoder with three SRM kernels. The SRM has proven effective in existing detection methods for image splicing forgery [16, 18, 20, 22]. The structure of the fixed SRM encoder is shown in Fig. 4. The SRM layer with the three SRM kernels obtains a noisy feature map through three channels from an RGB image. The noisy map is passed through three convolution layers, each with a kernel size of 5×5, a convolution stride of 2. Finally, the output feature of the fixed SRM encoder is down-sampled and simply fused with the output feature of the unfixed encoder. This fusion method is shown in Fig. 6-(a) and denoted as the

simple fusion method (SF).

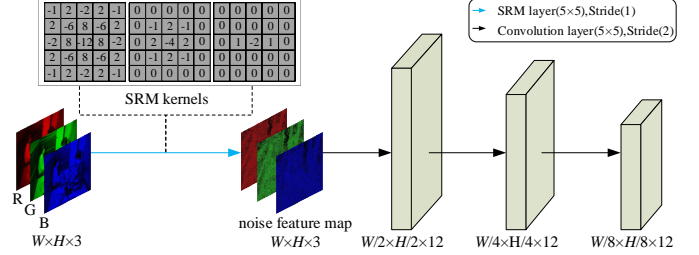


Fig. 4. Structure of the fixed SRM encoder.

We experiment on Unet-4-C and the fixed SRM encoder. The datasets and setting of parameters are the same as subsection III-A. The experimental results are listed in Table IV. The *F* score is slightly improved by additionally providing the image noise fingerprint to Unet-4-C. However, with the *Recall* rate increases, the *Precision* rate. This inverse relationship can be explained that, since Unet-4-C can autonomously learn the image noise fingerprint, the extra image noise fingerprint improved by the fixed encoder might simultaneously help and interfere with the learning of Unet-4-C, negating the final improvement. Therefore, providing a particular image fingerprint that can be autonomously learned by the networks maybe not a good way. How to effectively learn image fingerprints should be investigated more deeply in according to the intrinsic characteristic of image splicing forgery.

TABLE IV  
THE DETECTION RESULTS OF UNET-4-C WITH THE DIFFERENT FIXED ENCODERS ON CASIA AND COLUMB DATASET.

Method	Detection Result					
	CASIA		COLUMB			
	Precision	Recall	F	Precision	Recall	F
Unet-4-C	0.813	0.764	0.788	0.923	0.547	0.686
Unet-4-C SF The fixed SRM encoder	0.807	0.775	0.791	0.819	0.646	0.722
Unet-4-C SF The fixed DWT encoder	<b>0.824</b>	<b>0.782</b>	<b>0.803</b>	<b>0.906</b>	<b>0.651</b>	<b>0.757</b>

In most of the splicing forgery images, the tampered regions are objects with boundaries that introduce real edges. In this case, in addition to image fingerprints, the direction information of the pixels should be supplemented, since it represents the boundaries of the tampered regions. However, the direction information of the pixels is difficult to retain through the CNN processing. The direction information of pixels is additionally provided to the detection network, which may assist the detection network.

To test this idea, we perform a three-level Haar discrete wavelet transform (DWT) on each color channel of the input RGB image, which is shown in Fig. 5. Thirty-six (3×12) feature maps are obtained by the three-level wavelet decomposition (12 (3×4) feature maps at each level). The output feature of the fixed DWT encoder is fused with the output feature maps of the unfixed encoder by the simple fusion method (SF), as shown in Fig. 6-(a). The fixed DWT encoder was experimentally evaluated under the same conditions as the

fixed SRM encoder, and the detection results are listed in Table IV. All experimental results are improved from those of the fixed SRM encoder, confirming that the direction information of the pixels provided by the fixed DWT encoder assists the Unet-4-C in detecting and depicting the tampered regions.

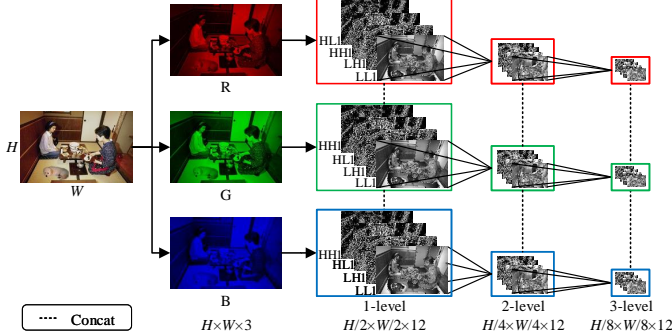


Fig. 5. Structure of the fixed DWT encoder.

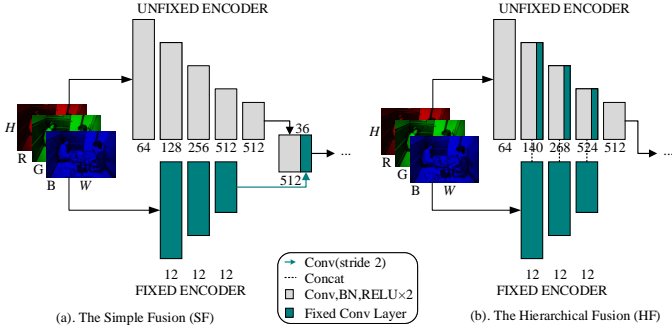


Fig. 6. Structures of the two concatenation methods: (a) simple fusion and (b) hierarchical fusion.

The above results confirm the effectiveness of providing the direction information of the pixels to Unet-4-C in the decoding process, but whether the direction information of the pixels can also assist Unet-4-C in the encoding process. For testing this idea, we propose a hierarchical fusion (HF) method between the fixed and unfixed encoder, which concatenates the output feature of each level in the fixed encoder to the output feature of the corresponding level in the unfixed encoder as shown in Fig. 6-(b). Unet-4-C is experimentally evaluated for different fixed encoders and concatenation methods (the datasets and setting of parameters are the same as subsection III-A). The detection results on the CASIA and COLUMB datasets are listed in Table V. In the UNet-4-C networks with the fixed SRM and DWT encoders, the HF improves the image-splicing forgery detection on both datasets (from that of SF). The direction information of the pixels provided by the fixed DWT encoder not only benefits the prediction of the detection network but also indicates the detection network where image fingerprints may be different in the encoding process. For a subjective analysis, the detection results of four splicing forgery images are shown in Fig. 7. Regardless of whether the tampered regions are similar to their neighboring regions (1<sup>st</sup> and 2<sup>nd</sup> columns in Fig. 7) or introduce obvious edges (3<sup>rd</sup> and 4<sup>th</sup> columns in Fig. 7), HF improves the

effectiveness of providing the direction information of the pixels in Unet-4-C.

TABLE V  
DETECTION RESULTS OF DIFFERENT CONCATENATION METHODS ON THE CASIA AND COLUMB DATASETS.

Method	Detection Result					
	CASIA			COLUMB		
	Precision	Recall	F	Precision	Recall	F
Unet-4-C SF The fixed SRM encoder	0.807	0.775	0.791	0.819	0.646	0.722
Unet-4-C HF The fixed SRM encoder	<b>0.835</b>	0.778	0.805	0.918	0.629	0.747
Unet-4-C SF The fixed DWT encoder	0.824	0.782	0.803	0.906	0.651	0.757
Unet-4-C HF The fixed DWT encoder	0.833	<b>0.794</b>	<b>0.814</b>	<b>0.926</b>	<b>0.648</b>	<b>0.763</b>

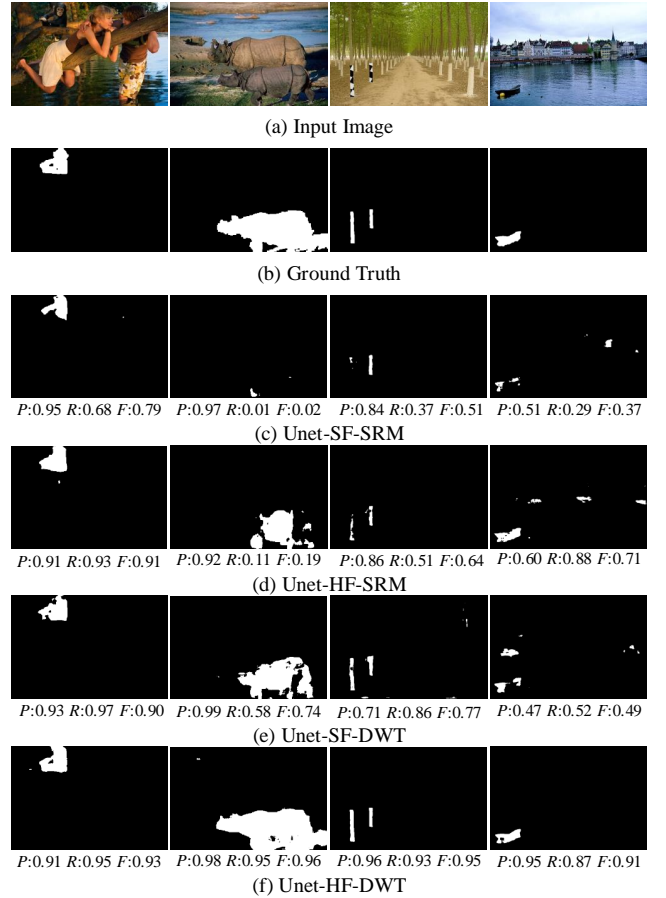


Fig. 7. Detected regions of four splicing forgery images, processed by Unet-4-C networks with different fixed encoders and different concatenation methods. Depicted are the forgery image (row a), ground-truth (row b), detection result of Unet-4-C with SF and the fixed SRM encoder (row c), detection result of Unet-4-C with HF and the fixed SRM encoder (row d), detection result of Unet-4-C with SF and the fixed DWT encoder (row e), and detection result of Unet-4-C with HF and the fixed DWT encoder (row f).

### C. Spatial Pyramid Global-Feature Extraction Module

In image splicing forgery detection, the tampered and non-tampered regions should be distinguished by a global binary classification. As shown in the fourth column of Fig. 9, one splicing forgery image contains multiple tampered regions

on different scales; therefore, the decision of the detection network must cross local regions and local objects. However, like the existing end-to-end detection networks [12–15, 20–22], the above network structure focuses only on local objects, which is insufficient for accurate detection of splicing forgery. For expanding the global perspective of the detection network further, we design a spatial pyramid global-feature extraction module (SPGFE) after the dual-encoder.

The SPGFE is inspired by human visual decision making. To observe a local part of an object, humans approach the object; to obtain a global view, they step away from the object. The proposed SPGFE module is shown in Fig. 8. The local feature maps generated by the fixed and unfixed encoders pass through three branches that generate global feature maps on different scales. The small-scale, medium-scale and large-scale global feature maps are concatenated and operated through a  $1 \times 1$  convolution layer, which outputs the final multi-scale global feature maps. The three convolution kernels with different sizes are equivalent to different viewing distances from an object.

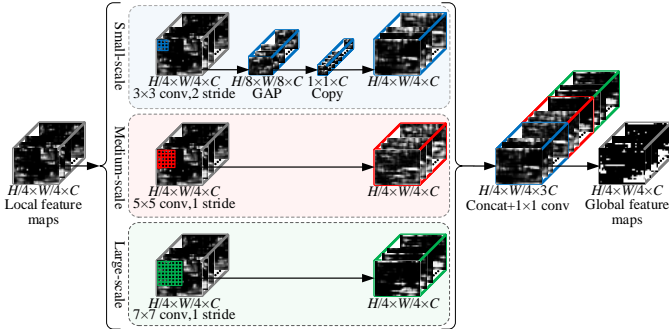


Fig. 8. Structure of the spatial pyramid global-feature extraction module.

The SPGFE module is experimentally evaluated on the dataset described in subsection III-A, under the same parameter settings. Various Unet-4-C configurations are tested: Unet-4-C combined with SPGFE (Unet-4-C-S), the fixed DWT encoder combined with Unet-4-C by HF (Unet-4-C-HF-FE), and Unet-4-C-HF-FE combined with SPGFE to expand the global insight (Unet-4-C-HF-FE-S). For a subjective analysis, five splicing forgery images are selected from the testing sets, and the detection results are shown in Fig. 9. The SPGFE clearly reduces the false detection rate and locates tampered regions of different sizes. As an objective evaluation, the detection results on the two datasets are listed in Table VI. The SPGFE undoubtedly improves the overall performances of the Unet-4-C and Unet-4-C-HF-FE detection networks.

Observing the complete set of analysis results in this section, the performance is optimized by cooperating with the fixed DWT encoder with Unet-4-C, fusing their feature maps by HF, and processing the local features of dual-encoder through the SPGFE module.

#### IV. EXPERIMENTS AND DISCUSSIONS

In this section, the performance of the proposed D-Unet is analyzed and evaluated in various experiments. Subsection

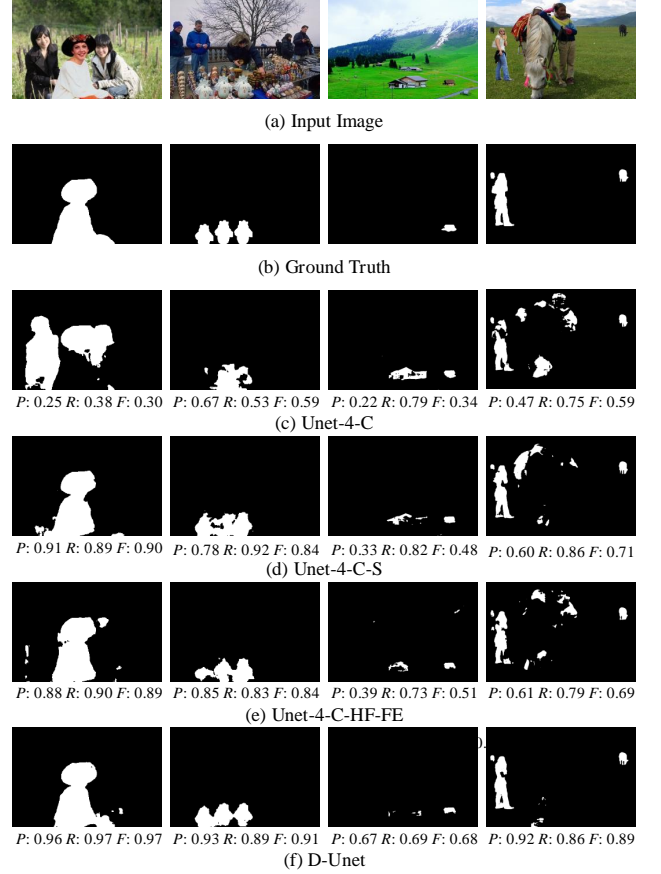


Fig. 9. Regions of five splicing forgery images, detected by Unet-4-C with and without the fixed DWT encoder and SPGFE. The 1<sup>st</sup>, 2<sup>nd</sup> and 3<sup>rd</sup> columns contain a tampered regions on different scales, respectively. The 4<sup>th</sup> column contains multiple tampered regions on different scales. Row a is the forgery image; row b is the ground-truth; row c is the detection result of Unet-4-C; row d is the detection result of Unet-4-C with SPGFE; row e is the detection result of Unet-4-C with the fixed DWT encoder (dual-encoder structure); row f is the detection result of dual-encoder network structure with SPGFE (D-Unet).

TABLE VI  
DETECTION RESULTS OF THE DETECTION NETWORKS WITH AND WITHOUT SPGFE ON THE CASIA AND COLUMB DATASETS.

Method	Detection Result					
	CASIA			COLUMB		
	Precision	Recall	F	Precision	Recall	F
Unet-4-C	0.813	0.764	0.788	0.923	0.547	0.686
Unet-4-C-S	0.833	0.817	0.825	0.941	0.701	0.803
Unet-4-C-HF-FE	0.833	0.794	0.814	0.926	0.648	0.763
Unet-4-C-HF-FE-S(D-Unet)	<b>0.866</b>	<b>0.852</b>	<b>0.859</b>	<b>0.96</b>	<b>0.901</b>	<b>0.93</b>

IV-A introduces the datasets and evaluation metrics used in the experiments. Subsection IV-B describes the implementation details and training process of D-Unet. Finally, subsection IV-C compares the effectiveness and robustness of D-Unet and several existing detection methods for image splicing forgery.

#### A. Experimental datasets and evaluation metrics

The image splicing forgery detection methods will be analyzed and evaluated on three public datasets, namely, CASIA [25], COLUMB [4], and NIST'16 [26]. The image information

of each dataset is detailed in Table VII. The CASIA dataset contains splicing forgery, copy-move forgery, and removal forgery. The tampered regions are carefully manipulated and post-processed by methods such as filtering and blurring, but no ground-truth masks of the tampered regions are provided. The CASIA dataset includes 5123 forgery images in TIFF and JPEG format. Most of the images have a resolution of 384×256. The COLUMB dataset contains 180 forgery images in TIFF format, with typical resolutions between 757×568 and 1152×768. This data includes only splicing forgery, and the tampered regions are the large meaningless smooth regions. The corresponding ground-truth masks are provided. The NIST'16 dataset is a challenging dataset containing 564 forgery images in JPEG format. The three types of local forgeries-splicing, copy-move, and removal-are included. The forgery images in this dataset have been post-processed to hide any visible traces of manipulation, and their corresponding ground-truth masks are also provided.

TABLE VII  
CHARACTERISTICS OF THE IMAGE SPLICING FORGERY DATASETS.

Dataset Name	Image Format	Ground Truth Mask	Forgery Region	Realistic	Forgery/Authentic Image
CASIA	TIFF, JPEG	No	Object	Yes	5123/7491
COLUMB	TIFF	Yes	Smooth	No	180/183
NIST'16	JPEG	Yes	Object	Yes	564/875

Because we aim to detect splicing forgery and localize the tampered regions, we select only the splicing forgery images in each dataset. The splicing forgery images from CASIA are randomly divided into 715 images for training, 35 images for validation, and 100 images for testing. The ground-truth masks of each image are handcrafted. The splicing forgery images from COLUMB are resized to 757×568 and randomly divided into 125 images for training, 10 images for validation, and 45 images for testing. Meanwhile, the splicing forgery images from NIST'16 are randomly divided into 184 images for training, 12 images for validation, and 50 images for testing. All images are resized to 512×384. Moreover, for verifying and estimating the robustness of the detection methods, we create various attack cases through JPEG compression, noise attack, and resize operation on the three testing datasets, as explained below.

- JPEG compression: the splicing forgery images are saved in JPEG format with different compression quality factors (QF).
- Noise attack: White Gaussian noises with a mean of zero and different variances are added to the splicing forgery images.
- Resize operation: the splicing forgery images are scaled using a ratio factor.

As the existing traditional detection methods are based on the compression property, they detect only JPEG images. Therefore, before running the comparison experiments, all experimental images in TIFF format are converted into JPEG format with a quality factor of 100%. The experimental images are listed in Table VIII.

TABLE VIII  
IMAGES USED IN THE EXPERIMENTAL SECTION.

	Name	Param	Range	Step	CASIA	COLUMB	NIST'16
Training	-	-	-	-	715	125	184
Validation	-	-	-	-	35	10	12
Testing	Original Images	-	-	-	100	45	50
	Plain	-	-	-	100	45	50
	JPEG Compression	QF	50-90	10	100×5	45×5	50×5
	Noise Addition	Var	0.002-0.01	0.002	100×5	45×5	50×5
	Resize Operation	Ratio	0.5-0.9	0.1	100×5	45×5	50×5
All Images		-	-	-	2450	900	1046

The performances of the methods for detecting image splicing forgery are evaluated by the *Precision*, *Recall*, and *F* rate. *Precision*, defined by Eq. (1), is the ratio of the correctly detected results to all detected results. *Recall*, defined by Eq. (2), is the ratio of correctly detected results to the ground-truth. In the image-level (pixel-level) evaluations, *TP* and *FP* denote the numbers of correctly detected and erroneously detected images (pixels), respectively, and *FN* is the number of falsely missed images (pixels). The *F* measure is the weighted harmonic mean of the *Precision* and *Recall* rate, and is given by Eq. (3).

$$Precision = \frac{TP}{TP + FP} \quad (1)$$

$$Recall = \frac{TP}{TP + FN} \quad (2)$$

$$F = \frac{2 \times Precision \times Recall}{Precision + Recall} \quad (3)$$

In the following experiments, *Precision*, *Recall*, and *F* are averaged over all images in each case.

### B. Implementation details and training process of D-Unet

In the pixel-wise classification by D-Unet, the network is followed by a sigmoid layer. Meanwhile, the agreement between the prediction mask  $p_i$  and ground-truth mask  $m_i$  corresponding to the  $i^{th}$  input  $x_i$  is measured by the cross-entropy (CE) loss. For  $N$  samples, the cross-entropy loss is computed as:

$$L_{loss} = \frac{1}{N} \sum_i ||m_i \log(p_i) + (1 - m_i) \log(1 - p_i)||_1. \quad (4)$$

D-Unet is trained using an Adam training optimizer [27] with an initial learning rate of  $3e^{-4}$ , a decay rate of 0, a batch size of 16, and an epoch of 50. All training processes are implemented on a NVIDIA Tesla V100 (32G) GPU. To evaluate the actual ability of the proposed D-Unet, we omit a pre-training method, and train the network on only hundreds of forgery images.

### C. Comparative experiments and analysis

This subsection compares the performances of the proposed D-Unet and several existing detection methods: color filter array (CFA) [28], noise inconsistency (NOI) [29], aligned double quantization (ADQ) [1], error level analysis (ELA) [30], U-shaped network (U-Net) [24], RRU-Net [15], ManTra [22], LSTM [21], coarse-to-refined network (C2RNet) [11], and FusionNet [19]. The details of each detection method are given in Table IX. All of these methods can detect tampered regions at the pixel-level. Some detection methods, such as those in [20] and [13], can judge only the type of forgery, so are excluded from the present comparison. The first four methods are based on traditional feature extractions. Their source codes were implemented and published by Zampoglou, *et al.* [31]. The remaining six detection methods are based on CNNs, and their source codes are provided by the authors. The hyperparameters of the detection networks are set to the values yielding the best performances in the original papers.

TABLE IX  
DETECTION METHODS COMPARED IN THE EXPERIMENTS.

Method	Description
ELA [30]	An error level analysis method, whose purpose is to find the compression error difference between the forgery regions and the real regions through different JPEG compression quality factors.
NOI [29]	A noise inconsistency-based method using high pass wavelet coefficients to model the local noises.
ADQ [1]	Aligned double quantization detection using the distribution of the image DCT coefficients.
CFA [28]	A CFA pattern estimation method, which uses the nearby pixels to approximate the camera filter array patterns and then produces the forgery probability for each pixel.
U-Net [24]	A good segmentation method, the network structure is a U-shape with concatenating the feature map between the same layer to achieve high-precision segmentation.
RRU-Net [15]	A ringed residual U-Net (RRU-Net) method, that is based on U-Net. The residual propagation and residual feedback modules are added to form a ringed residual structure, which improves the utilization of feature maps.
ManTra [22]	Two structures are utilized to classify forgery images and segment the forgery regions, two structures are image manipulation trace feature extractor (IMTFE) and local anomaly detection network (LADN).
LSTM [21]	A dual-domain detection method, an encoder-decoder structure is used in the spatial domain, the resampling features and LSTM networks are used in the frequency domain. After the two networks are integrated, the optimal effect is achieved.
C2RNet [11]	A two-stage detection method, including a coarse convolutional neural network (C-CNN) and a refined CNN (R-CNN), which learns the differences of the image properties between un-tampered and tampered regions from image patches with different scales.
FusionNet [19]	A deep fusion network concentrates learns the low-level forensic features and consequently detects the splicing forgery, the network is trained on a small automatically generated splicing dataset.

1) *Experiments of plain splicing forgery:* This subsection compares the performances of the proposed D-Unet and the other detection methods in detecting plain splicing forgery. A splicing forgery detection method must first correctly distinguish the splicing forgery image from the original image. Even CNN-based detection methods are not trained on the original image. To compare the image-level performances of the proposed D-Unet and other detection methods, we randomly select 195 forgery images and 195 original images from the CASIA, COLUMB, and NIST'16 datasets for testing. As some CNN-based detection methods cannot directly classify a forgery and its original image, the detection result  $F$  of the original image is below 0.05, but that of the forgery image exceeds 0.05. Such cases are regarded as classification errors. The image-level detection results are given in Table X. The proposed D-Unet outperforms the other detection methods, confirming that D-Unet correctly learns the different image fingerprints of the tampered and non-tampered regions. Although based on U-Net, D-Unet does not behave as a semantic segmentation network.

TABLE X  
EXPERIMENTAL RESULTS OF PLAIN SPLICING FORGERY AT THE IMAGE LEVEL.

Method	Year	Detection Result		
		Precision	Recall	$F$
ELA [30]	2007	0.514	0.719	0.599
NOI [29]	2009	0.543	735	0.625
ADQ [1]	2009	0.583	0.817	0.68
CFA [28]	2012	0.54	0.704	0.611
U-Net [24]	2015	0.663	0.846	0.743
RRU-Net [15]	2019	0.752	0.979	0.851
ManTra [22]	2019	0.677	0.805	0.735
LSTM [21]	2019	0.65	0.78	0.709
C2RNet [11]	2020	0.633	0.795	0.705
FusionNet [19]	2020	0.778	0.897	0.833
D-Unet	-	<b>0.787</b>	<b>0.985</b>	<b>0.875</b>

Besides distinguishing a forgery image from the original image, detection methods for splicing forgery images should accurately locate the tampered regions. The localization performances of D-Unet and the other detection methods are assessed by the *Precision*, *Recall*, and  $F$ . The performance values are listed in Table XI. The traditional detection methods yielded poorer *Precision* and  $F$  values than the CNN-based detection methods. The CFA, NOI, and ELA obtain very high *Recall* rates because they detect almost the entire image as the tampered regions. D-Unet outperforms the other CNN-based detection methods on the CASIA, COLUMB, and NIST'16 datasets, and is especially effective on the COLUMB dataset, possibly because (unlike the other methods) D-Unet extracts the directional information using a fixed encoder. Consequently, D-Unet effectively locates the large, meaningless smooth tampered regions. Note that the gap between D-Unet and FusionNet cannot be accurately measured because the

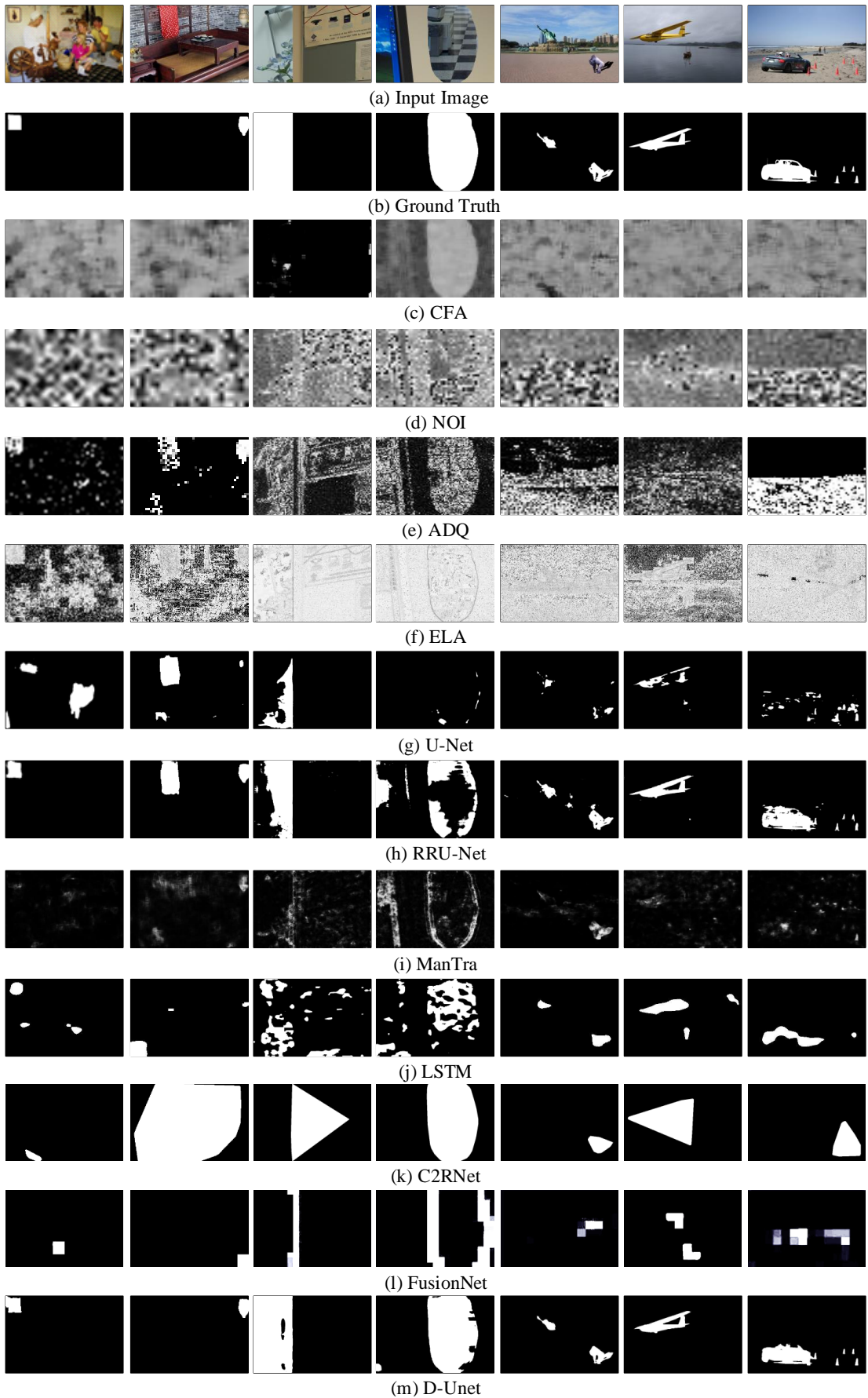


Fig. 10. Splicing forgery detection results of the proposed D-UNet and other detection methods. The forgery images are extracted from CASIA (1<sup>st</sup> and 2<sup>nd</sup> columns), COLUMB (3<sup>rd</sup> and 4<sup>th</sup> columns), and NIST'16 (5<sup>th</sup> and 6<sup>th</sup> columns). The forgery image in the 7<sup>th</sup> column shows an example of multiple tampered regions.

TABLE XI  
EXPERIMENTAL RESULTS OF PLAIN SPLICING FORGERY AT THE PIXEL LEVEL.

Method	Year	Detection Result								
		CASIA			COLUMB			NIST'16		
		Precision	Recall	F	Precision	Recall	F	Precision	Recall	F
ELA[30]	2007	0.086	0.975	0.158	0.316	0.961	0.475	0.141	0.922	0.315
NOI[29]	2009	0.149	<b>0.992</b>	0.258	0.422	0.997	0.593	0.202	<b>0.998</b>	0.336
ADQ[1]	2009	0.402	0.585	0.476	0.367	<b>0.998</b>	0.536	0.179	0.873	0.297
CFA[28]	2012	0.101	0.971	0.182	0.442	0.478	0.459	0.169	0.995	0.289
U-Net[24]	2015	0.815	0.735	0.773	0.906	0.535	0.661	0.803	0.631	0.707
RRU-Net[15]	2019	0.848	0.834	0.841	0.918	0.822	0.867	0.783	0.782	0.782
ManTra[22]	2019	0.821	0.793	0.807	0.856	0.849	0.852	0.816	0.824	0.82
LSTM[21]	2019	0.802	0.783	0.792	0.831	0.816	0.823	0.793	0.785	0.789
C2RNet[11]	2020	0.581	0.808	0.676	0.804	0.612	0.695	0.468	0.666	0.55
FusionNet[19]	2020	-	-	-	-	-	-	-	-	-
D-Unet	-	<b>0.866</b>	0.852	<b>0.859</b>	<b>0.96</b>	0.901	<b>0.93</b>	<b>0.863</b>	0.842	<b>0.852</b>

FusionNet method only detects the edges of the tampered region. Further subjective comparisons are shown in Fig. 10. Here, we show seven randomly chosen examples from the three datasets. Clearly, D-Unet obtains the best results among the comparison methods, even in multiple tampered regions with different scales in a forgery image.

2) *Experiments under various attacks*: To further verify the effectiveness and robustness of D-Unet, the performances of the proposed D-Unet and the existing detection methods are compared under various types of attacks: noise attack, JPEG compression, and resize operations. As the LSTM method [21] can only detect square images (such as 512×512- or 256×256-sized images), and the FusionNet method [19] can only detect the edges of a tampered region, these methods are excluded from the following experiments.

Adding noise to a tampered image is a general technique for hiding traces of the image manipulations. Therefore, an excellent forgery detection method should be sufficiently robust to noise attacks. In the first comparative experiment under an image noise attack, we estimate the robustness of D-Unet and the other detection methods to noise. The experimental results are shown in Fig. 11.

In Fig. 11, the *Precision*, *Recall*, and *F* scores are compared under noise attacks with different variances on images from the CASIA, COLUMB, and NIST'16 datasets. The detection performances of the four traditional detection methods are nearly equal. Although their *Precision* and *F* scores are lower than in the CNN-based detection methods, their *Recall* scores are elevated because traditional methods detect almost the entire image as a tampered region. Among the CNN-based detection methods, D-Unet usually achieves the highest *Precision* and *F*, but are slightly outperformed by RRU-Net on CASIA and COLUMB. D-Unet achieves higher *Precision* and *F* on NIST'16 than the other methods. This experiment demonstrates the promising robustness of the proposed D-Unet to noise attacks on all three datasets.

Image compression is very common in daily life. Compre-

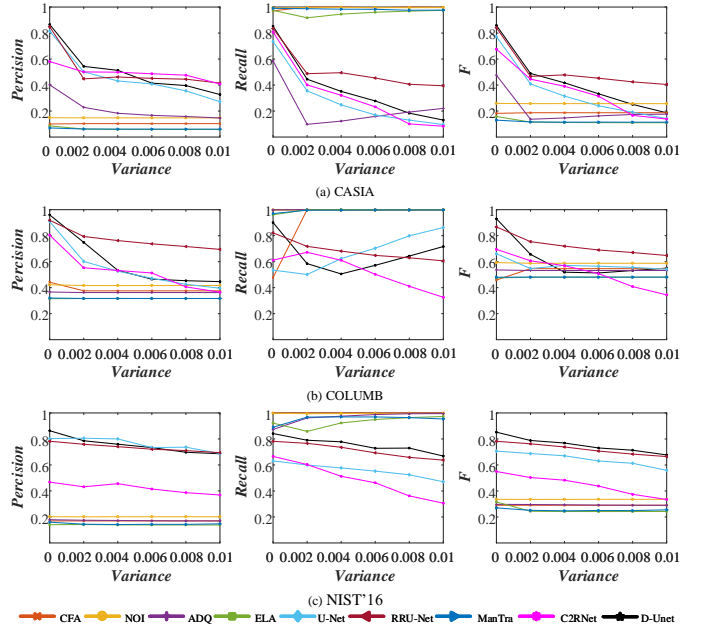


Fig. 11. Experiment results under the noise attacks. The first, second and third columns plot the *Precision*, *Recall*, and *F* scores, respectively. Rows a, b and c are the experimental results of the CASIA, COLUMB and NIST'16 datasets, respectively.

sion is applied to most of the images on the Internet, and is also a convenient means of hiding tampering traces. Therefore, we conduct a comparative experiment under a JPEG compression attack.

The *Precision*, *Recall*, and *F* scores of the different detection methods under JPEG compression attacks on images from the CASIA, COLUMB, and NIST'16 datasets are compared in Fig. 12. First, we find that a JPEG compression impacts the results of the CASIA images, but exerts very small impact on the results of the COLUMB and NIST'16 images. These outcomes might be related to the compositions of the different

datasets. The tampered regions of the COLUMB images are the large meaningless smooth regions, whereas the NIST'16 dataset contains many samples forged from the same or very similar base images. The particularity of the tampered regions in these two datasets might resist JPEG compression attacks. Second, when the quality factor decreases from 100 to 50, the *Precision*, *Recall*, and *F* of most of the detection methods descend dramatically, whereas the performance of D-Unet remains stable. Meanwhile, the CNN-based detection methods obtain higher *Precision* and *F* scores than the traditional detection methods, and D-Unet outperforms the other methods (similarly to the results under noise attack). In this experiment, the proposed D-Unet shows promising robustness under JPEG compression attacks on all three datasets.

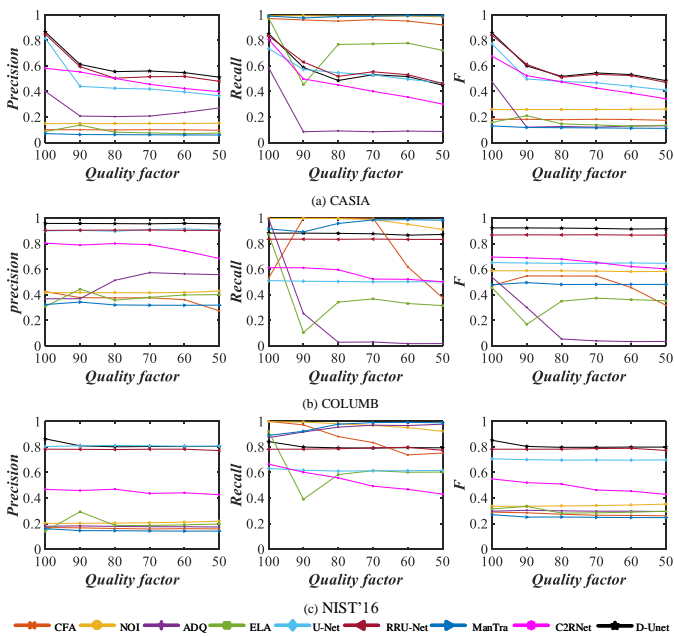


Fig. 12. Experimental results under JPEG compression attacks. The first, second and third columns plot the *Precision*, *Recall*, and *F* scores, respectively. Rows *a*, *b* and *c* are the experimental results of the CASIA, COLUMB, and NIST'16 datasets, respectively.

The resize operation provides a third way of hiding tampering traces. As the resize operation usually loses some pixels, it increases the difficulty of detection. Therefore, we also compare the performances of D-Unet and the existing detection methods under a resize attack.

The *Precision*, *Recall*, and *F* scores of the methods under resize attacks with different ratios on the CASIA, COLUMB, and NIST'16 datasets are plotted in Fig. 13. As indicated in the figure, D-Unet achieves higher *Precision* and *F* scores than most of the other methods, but is slightly outperformed by RRU-Net on the CASIA and NIST'16 datasets. On the CASIA dataset, D-Unet delivers better overall performance than the other detection methods, and is only slightly worse than RRU-Net at resizing ratios above 0.8. At ratios below 0.8, D-Unet consistently outperforms the other methods. On resized COLUMB images, D-Unet achieves higher *Precision* and *F* scores than the existing methods. This experiment confirms the robustness of the proposed D-Unet to resize attacks on all

three datasets.

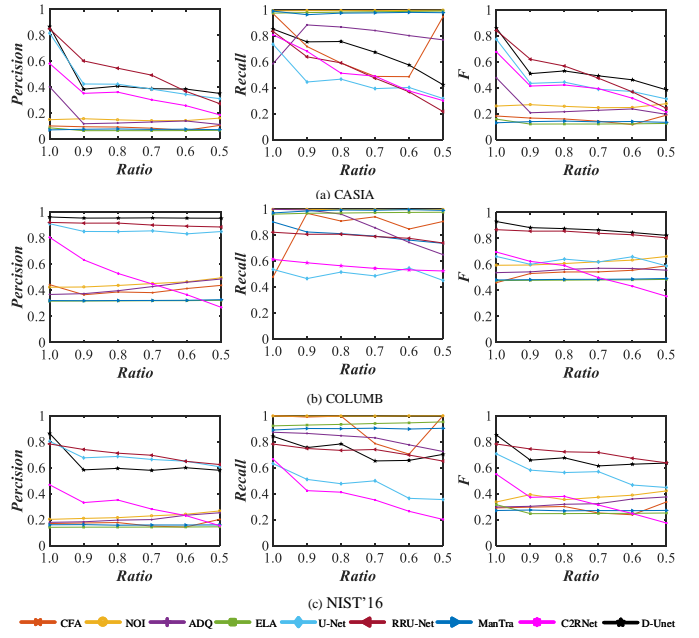


Fig. 13. Experimental results under the resize attacks. The first, second and third columns plot the *Precision*, *Recall*, and *F* scores, respectively. Rows *a*, *b* and *c* plot the experimental results of the CASIA, COLUMB and NIST'16 datasets, respectively.

## V. CONCLUSION

We have proposed an end-to-end dual encoder U-Net (D-Unet) for image splicing forgery detection, which can accurately locate the tampered regions without requiring pre- or post-processing. Owing to its structure, D-Unet gains a global insight into the image splicing forgery. D-Unet also maintains steady detection performance in different cases of splicing forgeries without requiring a large number of training samples or a complex pre-training process (the usual requirements of CNN-based detection methods). In a series of experimental comparison studies, D-Unet not only outperforms the state-of-the-art methods in image-level and pixel-level detection, but also presents more stable robustness under noise, JPEG compression, and resizing image attacks.

## REFERENCES

- [1] Z. Lin, J. He, X. Tang, and C.-K. Tang, "Fast, automatic and fine-grained tampered jpeg image detection via dct coefficient analysis," *Pattern Recognition*, vol. 42, no. 11, pp. 2492–2501, 2009.
- [2] M. K. Johnson and H. Farid, "Exposing digital forgeries in complex lighting environments," *IEEE Transactions on Information Forensics and Security*, vol. 2, no. 3, pp. 450–461, 2007.
- [3] S. Ye, Q. Sun, and E.-C. Chang, "Detecting digital image forgeries by measuring inconsistencies of blocking artifact," in *2007 IEEE International Conference on Multimedia and Expo*. Ieee, 2007, pp. 12–15.
- [4] Y.-F. Hsu and S.-F. Chang, "Detecting image splicing using geometry invariants and camera characteristics

consistency,” in *2006 IEEE International Conference on Multimedia and Expo*. IEEE, 2006, pp. 549–552.

[5] Z. Fang, S. Wang, and X. Zhang, “Image splicing detection using color edge inconsistency,” in *2010 International Conference on Multimedia Information Networking and Security*. IEEE, 2010, pp. 923–926.

[6] Z. Qu, G. Qiu, and J. Huang, “Detect digital image splicing with visual cues,” in *International workshop on information hiding*. Springer, 2009, pp. 247–261.

[7] M. Chen, J. Fridrich, M. Goljan, and J. Lukás, “Determining image origin and integrity using sensor noise,” *IEEE Transactions on information forensics and security*, vol. 3, no. 1, pp. 74–90, 2008.

[8] X. Pan, X. Zhang, and S. Lyu, “Exposing image forgery with blind noise estimation,” in *Proceedings of the thirteenth ACM multimedia workshop on Multimedia and security*, 2011, pp. 15–20.

[9] Y. Zhang, J. Goh, L. L. Win, and V. L. Thing, “Image region forgery detection: A deep learning approach.” *SG-CRC*, vol. 2016, pp. 1–11, 2016.

[10] Y. Wei, X. Bi, and B. Xiao, “C2r net: The coarse to refined network for image forgery detection,” in *2018 17th IEEE International Conference On Trust, Security And Privacy In Computing And Communications/12th IEEE International Conference On Big Data Science And Engineering (TrustCom/BigDataSE)*. IEEE, 2018, pp. 1656–1659.

[11] B. Xiao, Y. Wei, X. Bi, W. Li, and J. Ma, “Image splicing forgery detection combining coarse to refined convolutional neural network and adaptive clustering,” *Information Sciences*, vol. 511, pp. 172–191, 2020.

[12] M. C. Stamm and B. Bayar, “A deep learning approach to universal image manipulation detection using a new convolutional layer,” in *Proceedings of the 4th ACM Workshop on Information Hiding and Multimedia Security*, 2016, pp. 5–10.

[13] —, “Constrained convolutional neural networks: A new approach towards general purpose image manipulation detection,” *IEEE Transactions on Information Forensics and Security*, vol. 13, no. 11, pp. 2691–2706, 2018.

[14] R. Salloum, Y. Ren, and C.-C. J. Kuo, “Image splicing localization using a multi-task fully convolutional network (mfcn),” *Journal of Visual Communication and Image Representation*, vol. 51, pp. 201–209, 2018.

[15] X. Bi, Y. Wei, B. Xiao, and W. Li, “Rru-net: The ringed residual u-net for image splicing forgery detection,” in *Proceedings of the IEEE Conference on Computer Vision and Pattern Recognition Workshops*, 2019, pp. 0–0.

[16] Y. Rao and J. Ni, “A deep learning approach to detection of splicing and copy-move forgeries in images,” in *2016 IEEE International Workshop on Information Forensics and Security (WIFS)*. IEEE, 2016, pp. 1–6.

[17] J. H. Bappy, A. K. Roy-Chowdhury, J. Bunk, L. Nataraj, and B. Manjunath, “Exploiting spatial structure for localizing manipulated image regions,” in *Proceedings of the IEEE international conference on computer vision*, 2017, pp. 4970–4979.

[18] Z. Shi, X. Shen, H. Kang, and Y. Lv, “Image manipulation detection and localization based on the dual-domain convolutional neural networks,” *IEEE Access*, vol. 6, pp. 76 437–76 453, 2018.

[19] B. Liu and C.-M. Pun, “Exposing splicing forgery in realistic scenes using deep fusion network,” *Information Sciences*, 2020.

[20] P. Zhou, X. Han, V. I. Morariu, and L. S. Davis, “Learning rich features for image manipulation detection,” in *Proceedings of the IEEE Conference on Computer Vision and Pattern Recognition*, 2018, pp. 1053–1061.

[21] J. H. Bappy, C. Simons, L. Nataraj, B. Manjunath, and A. K. Roy-Chowdhury, “Hybrid lstm and encoder–decoder architecture for detection of image forgeries,” *IEEE Transactions on Image Processing*, vol. 28, no. 7, pp. 3286–3300, 2019.

[22] Y. Wu, W. AbdAlmageed, and P. Natarajan, “Mantranet: Manipulation tracing network for detection and localization of image forgeries with anomalous features,” in *Proceedings of the IEEE Conference on Computer Vision and Pattern Recognition*, 2019, pp. 9543–9552.

[23] J. Fridrich and J. Kodovsky, “Rich models for steganalysis of digital images,” *IEEE Transactions on Information Forensics and Security*, vol. 7, no. 3, pp. 868–882, 2012.

[24] O. Ronneberger, P. Fischer, and T. Brox, “U-net: Convolutional networks for biomedical image segmentation,” in *International Conference on Medical image computing and computer-assisted intervention*. Springer, 2015, pp. 234–241.

[25] J. Dong, W. Wang, and T. Tan, “Casia image tampering detection evaluation database,” in *2013 IEEE China Summit and International Conference on Signal and Information Processing*. IEEE, 2013, pp. 422–426.

[26] H. Guan, M. Kozak, E. Robertson, Y. Lee, A. N. Yates, A. Delgado, D. Zhou, T. Kheykhah, J. Smith, and J. Fiscus, “Mfc datasets: Large-scale benchmark datasets for media forensic challenge evaluation,” in *2019 IEEE Winter Applications of Computer Vision Workshops (WACVW)*. IEEE, 2019, pp. 63–72.

[27] D. P. Kingma and J. Ba, “Adam: A method for stochastic optimization,” *arXiv preprint arXiv:1412.6980*, 2014.

[28] P. Ferrara, T. Bianchi, A. De Rosa, and A. Piva, “Image forgery localization via fine-grained analysis of cfa artifacts,” *IEEE Transactions on Information Forensics and Security*, vol. 7, no. 5, pp. 1566–1577, 2012.

[29] B. Mahdian and S. Saic, “Using noise inconsistencies for blind image forensics,” *Image and Vision Computing*, vol. 27, no. 10, pp. 1497–1503, 2009.

[30] N. Krawetz and H. F. Solutions, “A picture’s worth,” *Hacker Factor Solutions*, vol. 6, no. 2, p. 2, 2007.

[31] M. Zampoglou, S. Papadopoulos, and Y. Kompatsiaris, “Large-scale evaluation of splicing localization algorithms for web images,” *Multimedia Tools and Applications*, vol. 76, no. 4, pp. 4801–4834, 2017.